

# 3D Pixel Mechanical Metamaterials

Fei Pan, Yilun Li, Zhaoyu Li, Jialing Yang, Bin Liu, and Yuli Chen\*

**Metamaterials have unprecedented properties that facilitate the development of advanced devices and machines. However, their interconnected building structures limit their applications, especially in the fields that require large deformation, rich programmability and efficient shape-reconfigurability. To break this limit and exploit more potentialities of metamaterials, an innovative material design strategy is proposed, named mechanical pixel (MP) array design. Similar to a screen that displays images by adjusting the colors of pixels, the metamaterials can form and reconfigure 3D morphologies by tuning the heights (lengths) of the MPs in the array. The strategy is demonstrated in a multistable metamaterial by experimental tests, theoretical analysis, and numerical simulations. Using this strategy, a large macroscopic shear deformation is obtained, and remarkable enhancements in the mechanical programmability, shape-reconfigurability and adaptability, and reusable shock-resistance are exhibited. Moreover, mechanical design and property prediction for the metamaterials are both greatly simplified due to the pixelated design. For a piece of the 3D pixel metamaterial with  $m \times n$ -unit MPs, the number of programmable displacement-force curves increases from  $n+1$  to  $2^{m+n+1}$ , and the number of stable morphologies grows from  $n+1$  to at least  $(n+1)^m$ . This strategy can be used to enhance the merits and further excavate the potential of versatile metamaterials.**

Mechanical metamaterials possess properties attributed to the rationally architected structures rather than the constituent materials and thus open a new door to create unprecedented properties and functions,<sup>[1–7]</sup> such as auxeticity,<sup>[5,8]</sup> negative compressibility,<sup>[9,10]</sup> shape-reconfigurability,<sup>[11,12]</sup> and programmability.<sup>[13,14]</sup> They are often constructed using periodically interconnected building blocks (also called “meta-atoms”) that

work collectively to exhibit macroscopic constitutive relations.<sup>[1,3]</sup> These connections among the meta-atoms endow the materials with definite shapes and stiffness to resist deformation. However, the kinematics of the meta-atoms are highly coupled and mutually constrained, and thus, large local deformation between the meta-atoms is hindered. In this case, even in the morphing metamaterials capable of large uniform macroscopic deformation, complex functional shapes with large local deformation, especially large shear deformation, cannot be formed. In addition, when encountering external loads, the passively induced shear deformation may lead to damage of the materials. Actually, high deformation flexibility and load-bearing robustness of the materials are of great importance and urgently needed in many applications, especially when the materials need not only to transform actively to adjust to circumstances but also to withstand extreme external loads, such as automotive armors, transformable robots, and morphing aircraft. Therefore, the means to gain more flexibility and robustness without sacrificing original performances poses a challenge for material and structure design.

To solve the problem, we propose an innovative strategy that is inspired by the spines of the hedgehog. Hedgehogs can erect their spines to threaten and stab predators. An additional function is to buffer the shock when falling from heights of more than 10 m.<sup>[15,16]</sup> Moreover, the damage to one spine rarely propagates to any other spines and thus prevents further destruction. The key point we can mimic is the array structure that is ubiquitous in nature, where the macroscopic deformation originates from the uncoupled deformations of the individuals. Mechanically speaking, by decomposing the macroscopic deformation into the motions of array modules and removing the redundant internal constraints, many hidden degrees of freedom (DOFs) can be released. Accordingly, we present a 3D pixelated design strategy to construct a type of mechanical metamaterial. Then, we demonstrate the concept in multistable metamaterials that have the merits of shape-reconfigurability, mechanical programmability, and reusable capability of energy absorption.<sup>[17,18]</sup> Meanwhile, inspired by the “flexible drinking straw,” which is a common gadget in daily life, we implement the design concept in an easily assembled prototype. By experimental tests, theoretical mechanics modeling, and numerical simulations, we can show that this bioinspired design strategy can greatly release the constrained DOFs of the building blocks

F. Pan, Y. Li, Z. Li, Prof. J. Yang, Prof. Y. Chen  
Institute of Solid Mechanics  
Beihang University (BUAA)  
Beijing 100191, China  
E-mail: yulichen@buaa.edu.cn

Prof. B. Liu  
AML  
CNMM  
Department of Engineering Mechanics  
Tsinghua University  
Beijing 100084, China

Prof. Y. Chen  
Department of Civil and Environmental Engineering  
Northwestern University  
Evanston, IL 60208, USA

The ORCID identification number(s) for the author(s) of this article can be found under <https://doi.org/10.1002/adma.201900548>.

DOI: 10.1002/adma.201900548

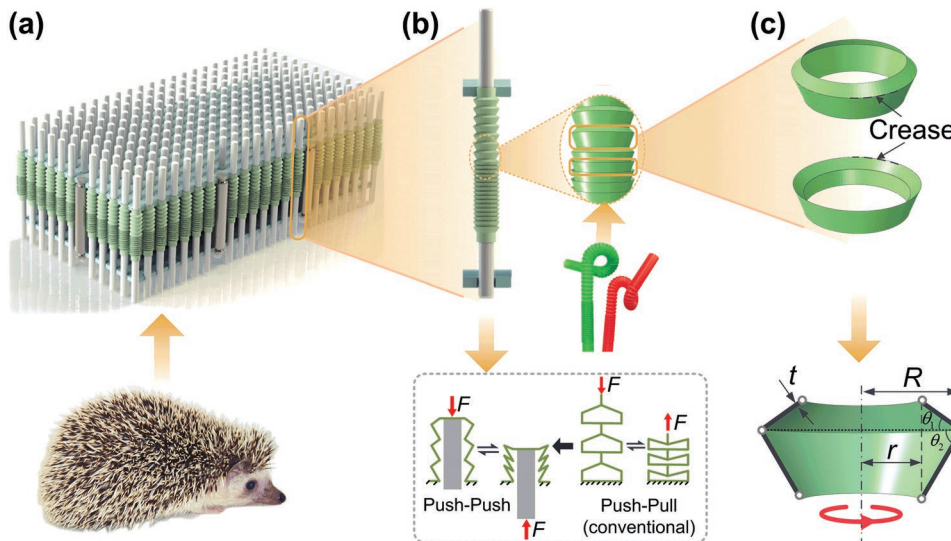


**Figure 1.** Schematic diagram of the design of 3D pixel mechanical metamaterial. a) The array-structured pixel metamaterial, which is inspired by the arrangement form of hedgehog spines (an African pygmy hedgehog (*Atelerix albiventris*) is illustrated here), is architected by parallel multistable MPs and a framework, and it can deform into various 3D shapes. b) The constituent MP is constructed of a hollow multistable structure and a guide bar connected through inside, and it can be loaded and reverse loaded both by push (compression). Inspired by the flexible drinking straw, the multistable structure is architected by crease-connected bistable units in series. c) The crease-connected truncated cone thin-wall structure has two stable states, i.e., deployed and retracted configurations. The sectional profile of the unit has five independent shape parameters.

and endow extremely large recoverable shear deformation compared to conventional bulk metamaterials,<sup>[11,19,20]</sup> thus significantly enhancing the deformability and exhibiting ultrarich programmability and shape-reconfigurability.

To thoroughly demonstrate the strategy, the newly designed metamaterials are expected to have two basic features. i) Their shapes and the mechanical properties can be actively tunable over an extended range, even after they are manufactured. ii) They can protect both the protected object and themselves from damage when encountering extreme external loads and can recover from distortion and reuse with minimal or zero maintenance. Similar to the arrangement of hedgehog spines (Figure 1a) and other biological array structures, we propose an array architecture design composed of parallel pillars. Periodically assembled in a patterned framework, these pillars should have the characteristics of morphing and absorbing mechanical energy. One of the most excellent candidates with these properties is the multistable element architected by bistable units in series (Figure 1b).<sup>[18]</sup> It can switch among its multiple stable shapes and absorb energy via fully reversible elastic deformation.<sup>[17,19–21]</sup> Moreover, it has a greater tunable mechanical response, larger deformation amplitude, and a greater number of stable shapes compared to other strategies, such as shape memory material<sup>[22,23]</sup> and foldable origami.<sup>[24–26]</sup> Therefore, the mechanical multistable element is adopted here. To guarantee the kinematic decoupling and the load capability of the pillars, only the axial deformation is allowed because bending is generally inefficient in load-bearing. Thus, the metamaterials can deform without shear constraint and present abundant 3D configurations. Note that the pillars in the array are very similar to the pixels on a screen, i.e., the former form 3D morphologies by varying heights (lengths) while the latter display 2D images by tuning colors. Thus, we define these pillars as mechanical pixels (MPs).

To realize the multistable MP, we should reconsider two factors. i) The deformation can be guided. The MP should have high bending rigidity to avoid transverse deformation and should also have sufficient axial compliance to transform among different stable shapes. ii) The efficiency and convenience of the morphing and reusability should be enhanced. For example, the MP can easily recover to a working condition after distortion. Therefore, a hollow multistable structure connected with a guide bar through the inside is designed (Figure 1b). The push–pull loading–reverse loading mode is thus changed to a push–push mode (Figure 1b; Movie S2, Supporting Information), making the materials able to work continuously and efficiently when served as energy absorbers because the most common loading type of impacts and collisions is compression. For the hollow multistable structure, we adopt a thin-wall structure inspired by the “flexible drinking straw” (Figure 1b). It is composed of crease-connected circular truncated cones. As the meta atom, the basic unit of the straw-like structure has two required stable states, deploy and retract (Figure 1c), and it can be described by five independent geometry parameters. These are the outer and inner diameters  $R$  and  $r$ , the truncated cone angles  $\theta_1$  and  $\theta_2$ , and the thickness of the wall  $t$  (Figure 1c), which will be discussed later. The connecting creases can be constructed using hinges composed of plastic, metal, or other materials.<sup>[11,27,28]</sup> In brief, all the multistable MPs are aligned in parallel with one end connected to the bar and the other end connected to the framework (Figure 1a,b; Supporting Information) and can deform and carry an axial load independently (the bending of the straw-like structure is restrained by the guide bar). In this work, we fabricated a prototype with 187 MPs made of commercial polypropylene (PP) flexible drinking straws to materialize the concept experimentally (Supporting Information). Each straw structure consists of 60 bistable units and

is approximately 50 mm long when completely retracted and approximately 105 mm long when fully deployed (Figure S13, Supporting Information). The MPs are arranged in the pattern of a triangular honeycomb (Figure S14, Supporting Information).

As the meta atom of the material, the circular truncated cone thin-wall structure is expected to be bistable. The axial force under displacement loading is analyzed by an energy-based mechanics theoretical method and simulated by the finite element method (FEM) (see details in the Supporting Information). The compression loading is performed on a unit with  $R = 3.18$  mm,  $r = 2.67$  mm,  $\theta_1 = 44^\circ$ ,  $\theta_2 = 70^\circ$ , and  $t = 0.15$  mm, in accordance with the parameters of the experimental samples. Both the theoretical analysis and the numerical simulation captured a smooth "N"-shaped curve with two stable states and two extrema of force at the peak and valley, which are denoted as  $F_{\max}$  and  $F_{\min}$ , respectively (Figure 2a; Movie S1, Supporting Information). In addition, if the unit is loaded by a force boundary, snap-through may occur when the curve enters the negative stiffness regime at the peak or valley (dashed line in Figure 2a), which can form a hysteresis loop. Similarly, the multistable "straw structure" should also theoretically possess such a hysteresis loop.<sup>[17,18]</sup> To characterize this feature of the multistable MP, we utilized a servo-electrical MTS frame (E44.104, MTS) to test the axial mechanical response of a sample which is also fabricated of the same flexible drinking straw (Supporting Information). The loading was started from the fully deploying state with zero stress. The load first increased to 15 N and then decreased to -15N, and then repeated. The loading-reverse loading cycling shows the expected hysteresis loop which is theoretically well-predicted (Figure 2b). With the increase in displacement, the load on the multistable MP increases in the initial regime before reaching the same strength  $F_{\max}$  as its bistable components and then turns into a plateau instead of entering the negative stiffness regime, eventually growing steeply when all the units are retracting. Reverse loading also behaves in the same way. In addition, after 30 cycles, the hysteresis loop almost maintains the same profile (Figure S24, Supporting Information), demonstrating excellent reusability.<sup>[17,18]</sup>

Due to their multistability, the MPs have multiple stable lengths, where each length corresponds to a unique loading curve (see details in the Supporting Information). Taking the fully deployed or retracted state as the reference configuration, the MP can be precompressed or pretensioned to a certain stable length (Figure 2c,d). The loading/reverse loading on the precompressed/tensioned MP still behaves on a similar curve as the full-length one, which has the same plateau force and the steeply growing stage (Figure 2c). Thus, the curve can be tuned by adjusting the initial length. Considering an MP with  $n$  identical bistable units, it has  $2^n$  stable states and  $n+1$  stable lengths, resulting in  $n+1$  different displacement-force curves. For a length which requires  $l$  of the  $n$  units to be retracting, there are  $n!/[l!(n-l)!]$  eligible stable states. For example, except for the minimum/maximum length (all units are either retracted or deployed), each stable length has more than one eligible stable state (Figure 2d).

When pressing the metamaterial, the contact pressure is the resultant force of the MPs on a unit area, which can be obtained

by linear superposition due to the uncoupled deformation. Thus, adjusting the area density of MPs can tune the effective contact pressure. By designing the arrangement pattern and density of MPs on the supporting framework (Figure 1a), we can perform a preliminary programming of the effective contact pressure. Furthermore, we can adjust the initial length of the MPs to generate predefined stairs, which changes the MP area density distribution along the loading direction, and thus, we can program the displacement-force curve (Figure 2e). Taking the metamaterial with  $m$  MPs as an example, when compressed by a rigid flat plate (Figure 2e), the total loading curve is a superposition of the loading curves of the  $m$  MPs, which can be programmed by allocating the initial length of these MPs. Figure 2f illustrates the programmable space of the displacement-force curves and five typical loading curves of a metamaterial with  $n = 60$ . When all the MPs are initially fully deployed or retracted initially, we can obtain two bounds of the loading curves. Between the two bounds, there is the programmable space in which we can design arbitrary monotonic curves from the starting point A to the ending point B by designing specific stairs. For example, we can get a linear curve by setting a uniform distribution for the number of MPs with respect to different initial lengths. In addition, there is an expanded space for the program of initial stiffness, ranging from a lower bound with nearly zero stiffness to the steepest upper bound. Theoretically, there are at most up to  $n+1$  stairs (equal to the number of stable lengths) that we can set. Thus, we can obtain  $(n+m)!/(n!m!)$  different loading curves (see details in the Supporting Information). If considering the difference between loading and reverse loading curves, the number of curves can even be doubled as  $2(n+m)!/(n!m!)$ . It is also noted that the same loading curve may originate from different rearrangements, as the relation between the lengths and stable states of a single MP. In addition, the loading and reverse loading curves for three typical predefined stairs were tested experimentally by using a flat plate (Figure 2g). Without any precompression/tension on the MPs (Figure 2g(I)), the curve presents a shape similar to that of a single MP (Figure 2b). Then, we precompressed/tensioned the 42 MPs for approximately 25 mm (Figure 2g(II)) and obtained a curve with two plateaus, which initially can provide a softer cushion in the energy-absorption process. By precompressing/tensioning 42 of the 187 MPs to their final stable states (Figure 2g(III)), the curve presents a lower plateau, which reduces the maximal effective stress and can be used to protect objects with relatively lower strength. It is found that the oscillation in the plateau regime of a single MP (Figure 2b) is smoothed by the superposition. Additionally, the initial stiffness and plateau force are reduced by the superposition of potential defects. This feature endows the materials with the capability to analogize a category of material constitutive with increasing or zero tangential stiffness (Figure 2e,f), especially when  $m$  and  $n$  are large. Using this strategy, we can not only design the initial stiffness but can also program the displacement-force curves starting from a zero force, which is different from the metamaterials whose programmable stiffness originates from compressed/stretched states with nonvanishing external loads.<sup>[29]</sup> Note that the metamaterial in this work consists of identical MPs which are architected using the same units for the convenience of manufacturing. To gain more functional properties,

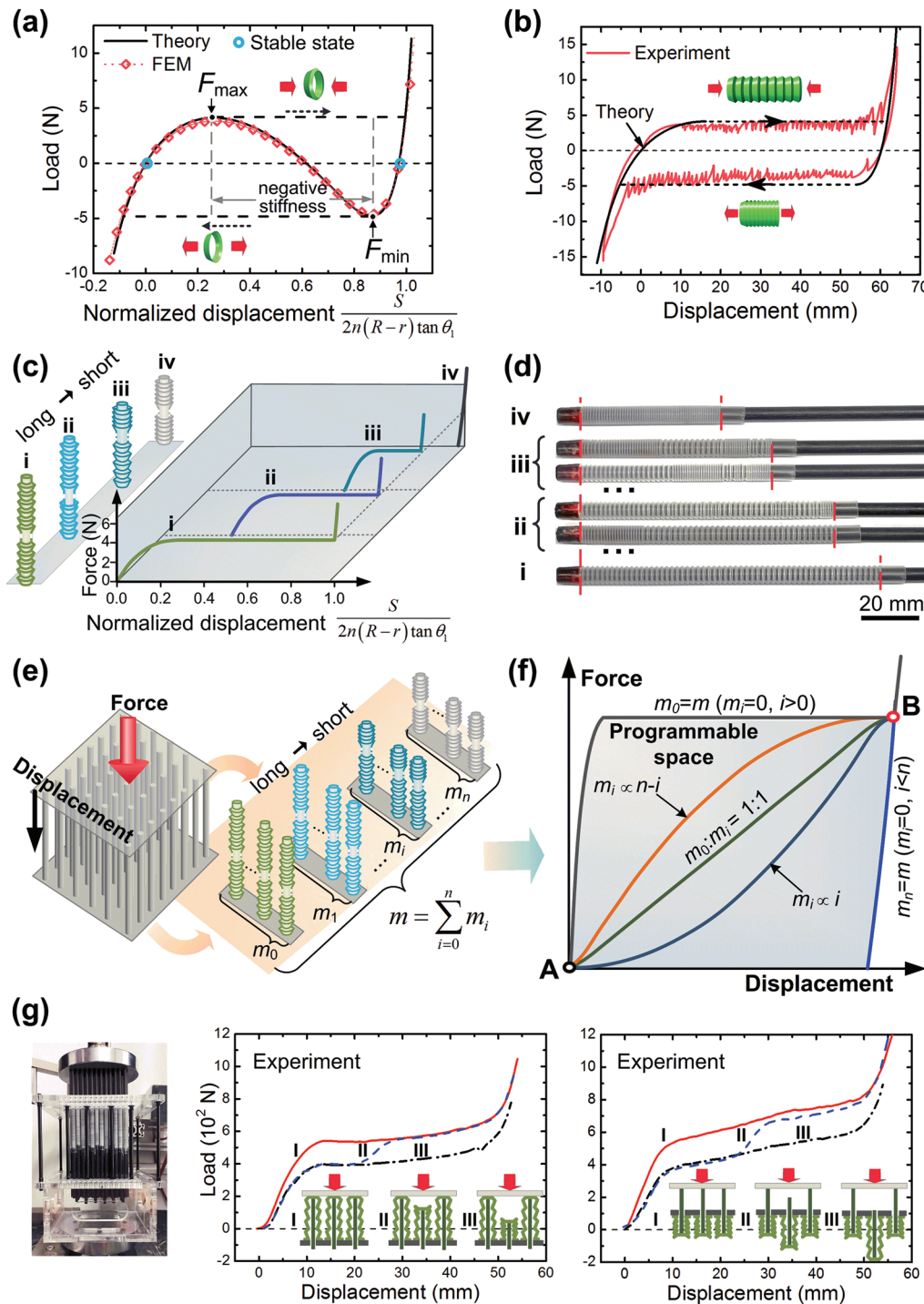


**Figure 2.** Mechanical behavior of the bistable unit, multistable MP, and 3D pixel mechanical metamaterial. a) The “N”-shaped curve of displacement boundary loading and the two stable states of the bistable unit are obtained from an energy-based mechanics theoretical analysis and numerical simulation by FEM. Snap-through occurs at the peak (valley) when the curve is entering the negative stiffness regime if the unit is loaded by a force boundary. b) Experimental results of the cycling loading of the multistable MP made of flexible drinking straw. c) The loading curve of one multistable MP can be tuned by adjusting the initial length. All the curves have the same plateau force and steeply growing stages but different initial elastic regimes. d) Photograph of the multistable MPs with four different typical lengths. Except for the minimum/maximum length (all units are retracting/deploying), each length has more than one eligible stable state. e) Schematic diagram of the strategy of programming the loading curve by adjusting the distribution of initial length of MPs. The total loading curve of the metamaterial is a superposition of the curves of all the MPs. f) Programmable space and typical loading curves of the 3D pixel metamaterial obtained by different predefined stairs where the unit number in one MP is 60. In the programmable space, an arbitrary monotonic curve from the starting point A to the ending point B can be obtained. g) Experimental results of loading and reverse loading for the metamaterial with three predefined stairs.

spatial gradients of the units can also be introduced to the design. For example, the shape parameters of the units can be varied in an MP, and the MPs in the same piece of material can also differ. Therefore, the number of programmable loading curve of the material can be further enlarged to a huge space of at the most  $2 \times 2^{m \times n}$ , where each stable state can correspond to two different loading curves (loading and reverse loading).

In addition to actively tuning their shape to program the loading curve, the metamaterials can also be actively morphed to adapt to different environments and applications. On the same piece of metamaterial, we can repeatedly sculpt configurations with arbitrary shapes. For example, the characters with sudden height variations on the edge (for which the macroscopic shear strain is extremely large) (**Figure 3a**) can easily be created on the metamaterial, which is still hard to form in bulk materials.<sup>[11,20]</sup> Nonplanar shapes with continuous height variation but sharp edges and corners can also be sculpted, as in the “pyramid” in Figure 3a. In addition to these convex shapes, concave configurations are also achievable, as in the convex and concave “heart” shown in Figure 3a. More importantly, the configurations of the metamaterials can be retained and even remain unchanged under certain external loads due to the multistability. Considering a piece of the metamaterial composed of  $m$  multistable MPs that all have  $n$  bistable units, the number of stable states theoretically reaches the enormous number of  $2^{m \times n}$ , greatly enriching the morphologies. If only the axial length variation is considered, the  $m$  MPs, which all have  $n+1$  stable lengths, can contribute to construct  $(n+1)^m$  surface morphologies for the material, which is much greater than that of the bulk material.

The deformability and multistability of the MPs can protect objects without subsequent damage to the MP structure itself. Due to the independence of the MPs, the deformation of one MP is only determined by the indentation depth of the contacted point. Thus the surface of the metamaterial can perfectly fit the profile of the object (Figure 3b). In other words, it can adapt to the shape of the contacted object, especially when the surface is nonplanar. In addition, there is no macroscopic Poisson’s effect or shearing for a nonplanar contact.<sup>[30]</sup> The stress condition is much simpler than that of continuum materials and thus severe stress concentration can be avoided. Therefore, both the object and the metamaterial can be well protected, especially when contacting sharp edges or corners. Furthermore, the deformed materials can retain the profile of an object even after removing it (Figure 3b). This can be used to recall the impact scene.

To verify visually the protection capability of the metamaterial, dynamic impact experiments by free-falling plaster “golden eggs” down to the metamaterial were conducted (Figure 3c; Movie S3, Supporting Information). To make a comparison, we prepressed all the MPs to the final stable states and skipped the plateau regime, causing the metamaterial to lose almost all its energy absorption capability. The results show that the “golden egg” can be well protected by the metamaterial with a long range of plateau loading force (Movie S3, Supporting Information). Furthermore, due to the merits of shape-adaptivity and shape-memory, a shape-fitting pit is formed on the metamaterial to hold the convex golden egg steady, which can effectively prevent it from toppling. To discuss the protection capability

in greater depth, we make contrast simulations under a more severe loading case. Drop tests of a tilted slender rectangular object with sharp corners are simulated by FEM. The 3D pixel metamaterial can catch the object steady and smoothly, without damage to the material or the protected object (Figure 3d(i); Movie S4, Supporting Information). After this process, the deformed MPs can be recovered and further reused (Figure 3e). As a sharp contrast, the arrays with moderate mutual constraints (Figure 3d(ii)) and conventional bulk materials with the same mechanical responses (Figure S19, Supporting Information; Figure 3d(iii)) cannot successfully protect the object and even themselves (Movie S4, Supporting Information). In the latter two cases, the rectangular object topples over during the dropping process. Moreover, it is found that due to the coupling of deformation, the stresses on the object are much larger in the latter two cases (Figure 3f), which can damage the bulk material due to large shear deformation. Therefore, if this multistable array concept is realized with appropriate materials and size, this strategy could be applied in reusable energy absorbers for car accidents and aircraft crashes and in stable landing cushions for recyclable spaceships and rockets.

The macroscopic performance of the metamaterial is determined by the arrangement, initial morphology, and intrinsic properties of the bistable unit. Moreover, the macroscopic mechanical response can be designed and obtained by superposition based on the responses of the units with no need for additional macroscopic mechanics analysis, which creates a simple “unit-based mechanical design” concept. Therefore, the essentials of the macroscopic mechanical behavior are determined by the displacement–force curve of the bistable unit which can be tuned by changing its shape parameters and elastic constants. To obtain a dimensionless relation for the bistable unit, we introduce the strain  $\varepsilon$  and normalized effective stress  $\hat{\sigma}$  of the unit, defined as

$$\varepsilon = \frac{S}{(R-r)(\tan \theta_1 + \tan \theta_2)} \quad (1)$$

$$\hat{\sigma} = \frac{F}{\pi t(R+r)E} \quad (2)$$

where  $E$  is the Young’s modulus of the material of the unit, and  $F$  and  $S$  are the force on and displacement of the unit, respectively. With the variation in the shape parameter, besides the bistable mode, two monostable modes of the strain–stress curve of the unit are captured by FEM simulations (Supporting Information), as illustrated in **Figure 4a**, i.e., the snap-through mode and the monotonic mode. For the former, the valley force  $F_{\min} > 0$ ; thus, the unit only has one stable state and loses the bistability for programming and shape-reconfiguration. However, the negative stiffness regime can still maintain a hysteresis loop. Thus, this feature can be applied in a self-recovery energy absorber.<sup>[20]</sup> The latter one loses its negative stiffness regime and hysteresis loop, thus should be avoided in design. The phase diagrams for the three modes are plotted with the parameters  $(\theta_1, \theta_2)$  (only  $\theta_1 < \theta_2$  are investigated due to their symmetry), as shown in **Figure 4b,c**. The results show that reducing  $\theta_1$  can lift the valley stress from negative to positive

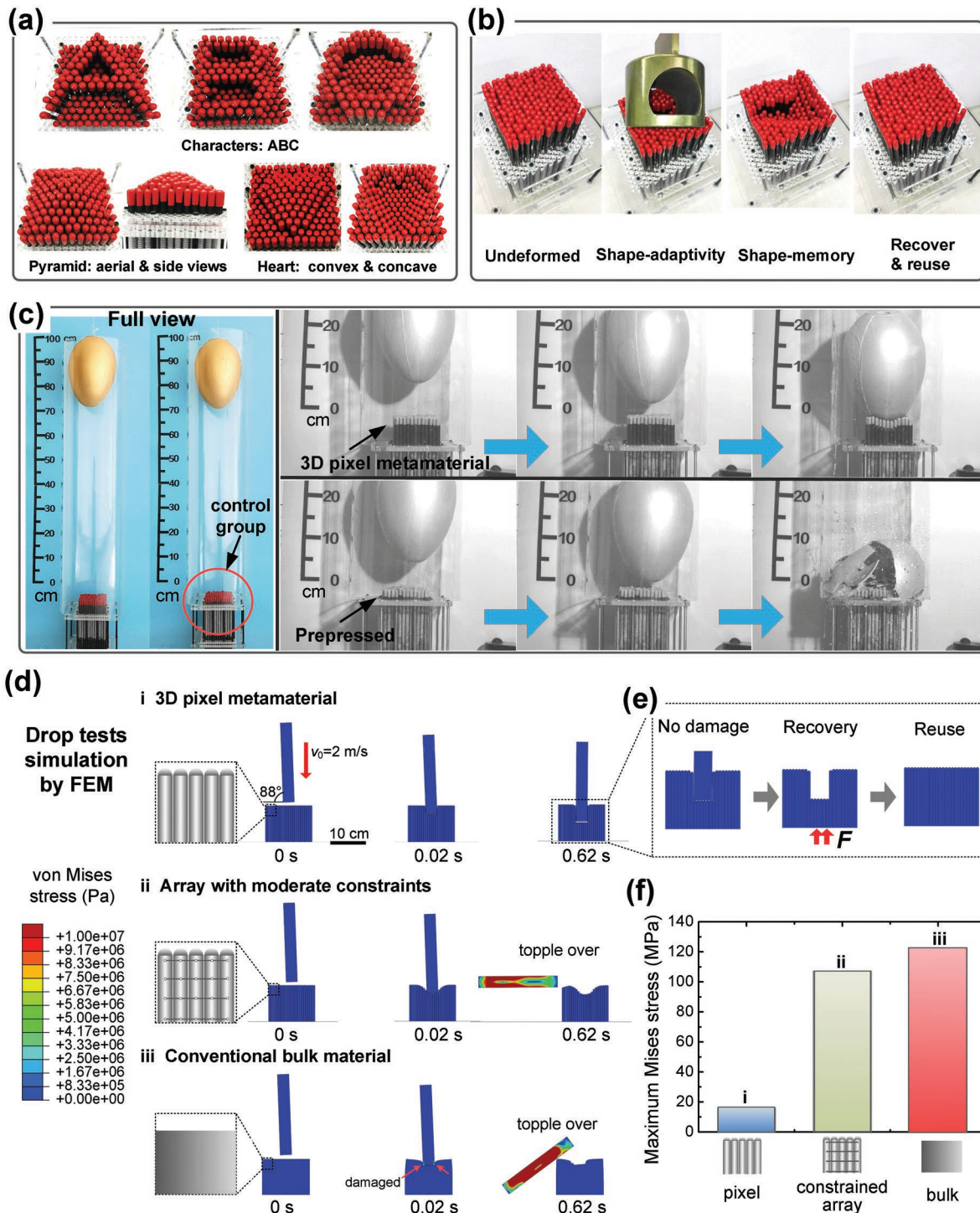


**Figure 3.** Shape-reconfigurability and shock protection of the 3D pixel mechanical metamaterial. a) The same piece of metamaterial can be reconfigured into characters with sharp edges and both convex and concave geometrical shapes with continuous height variation. To enhance the visual effect, a red rubber cap is placed on the end of each guide bar. b) The metamaterial can fit the shape of the nonplanar protected object and reserve the profile even after removing it, and it can then be fully recovered and reused. c) Tests of free-falling plaster “golden eggs” falling down to the metamaterial. The metamaterial can effectively protect the golden eggs from breakage and also provide an additional stable support during the process. As a contrast, the golden eggs that fell from the same height broke when contacting the fully prepressed metamaterial. d) Simulations of the drop test of a tilted rectangle with the 3D pixel metamaterial, array-structured material with moderate constraints, and a bulk material with the same mechanical properties. The 3D pixel metamaterial can fit the shape of the object and effectively protect it from damage and toppling. e) The 3D pixel metamaterial can be recovered and reused after a task execution. f) The maximum von Mises stress in the rectangular object during the dropping process for the three cases, in which the lowest one indicates the best protection.

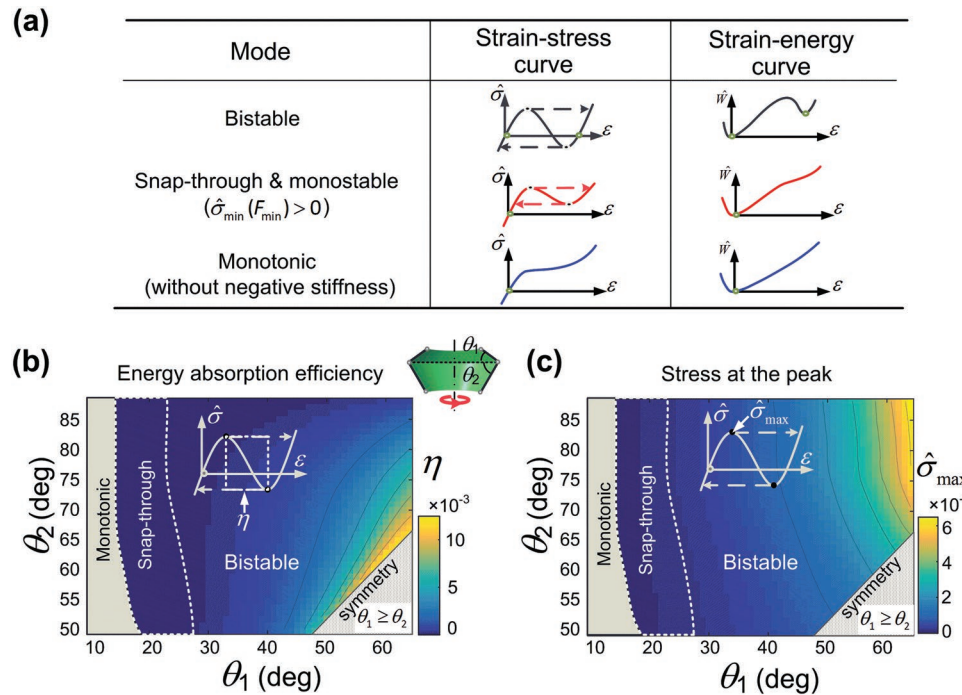


**Figure 4.** The influence of shape parameters on the performance of bistable unit. a) Three strain–stress curve modes of the unit. b,c) Phase diagrams and contour maps for the normalized energy-absorption efficiency  $\eta$  (b), and stress at the peak  $\hat{\sigma}_{\max}$  (c), with respect to the angles  $\theta_1$  and  $\theta_2$ .

and further cause the strain–stress curve to become monotonic. Therefore, the parameters should be selected carefully in these regimes. In addition, a dimensionless evaluation of the energy absorption efficiency  $\eta$  can be defined as

$$\eta = (\hat{\sigma}_{\max} - \hat{\sigma}_{\min})(\varepsilon_{\min} - \varepsilon_{\max}) \quad (3)$$

where the subscripts “max” and “min” represent the peak and valley values, respectively.  $\eta$  is the dimensionless energy density of a rectangular area in the hysteresis loop (the inset in Figure 4b). The scaling relations of these dimensionless factors with respect to shape parameters are investigated by FEM (see more details in the Supporting Information) based on the shape parameters taken in Figure 2 and illustrated by the contour maps in Figure 4b,c. The results show that both increasing  $\theta_1$  and reducing  $\theta_2$  can produce higher energy absorption efficiency (Figure 4b). In addition, a larger amplitude of  $\hat{\sigma}_{\max}$  ( $F_{\max}$ ) tends to exist in the regime with larger values of  $\theta_1$  and  $\theta_2$  (Figure 4c), while  $\hat{\sigma}_{\min}$  ( $F_{\min}$ ) with a larger amplitude favors larger  $\theta_1$  and smaller  $\theta_2$  (Figure S10, Supporting Information). Based on the parametric investigation, the strain–stress curve can be optimally designed, which lays a solid foundation for the design of metamaterials.

Compared to the multistable mechanical metamaterials and structures constructed by interconnected building blocks,<sup>[11,19,20,31,32]</sup> the pixelated array design strategy unties the coupled DOFs in bulk materials and releases a tremendous number of hidden stable states, which greatly improve the programmability and deformability. The number of programmable loading curves increases from  $n+1$  to  $2(n+m)!/(n!m!)$ , and the number of stable morphologies grows from  $n+1$  to  $(n+1)^m$ . In addition, highly nonuniform macroscopic deformation

can be easily presented through the guided deformation mode of the building blocks without distortion or destruction, which is yet hard to realize in bulk metamaterials. Therefore, when actively or passively forming complex configurations, the possibility of damage can be reduced. In addition, due to the decoupled motions of the MPs, the macroscopic mechanical response of the material is totally inherited from the basic meta atoms and thus can be designed and obtained solely by linear superposition rather than additional macroscopic mechanical analysis. It is also noted that the metamaterial is not limited to the design presented in this paper. The strategy we introduce here also applies to other multistable MPs with different architected structures,<sup>[11]</sup> bistability realization methods<sup>[31,32]</sup> or materials.<sup>[29,33]</sup> Additionally, it can be applied in material systems with active morphing strategies controlled by chemicals,<sup>[34]</sup> electric fields,<sup>[35]</sup> magnetic fields,<sup>[12]</sup> etc. Although the prototype we fabricated in this work is on the centimeter scale, the strategy we proposed can be extended to miniaturized structures, which can be further used to construct laminate or membrane mechanical metamaterials with 2D characteristic sizes. The framework can also be deformable and flexible, thus the materials can find more applications, such as soft machines and biomechanical devices.

In summary, we have proposed a novel strategy to construct a type of multistable mechanical metamaterial with greatly enhanced stiffness programmability, shape-reconfigurability, and shock-protective capacity. These are demonstrated by experiments, energy-based mechanics theoretical analysis, and FEM simulations. This concept can be used to design and fabricate versatile metamaterials or metastructures for many applications, ranging from transformable machinery and robots, to reusable energy absorbers for car accidents and stable landing

cushions for recyclable spaceships and rockets, and to material constitutive simulators and mechanical information preservation devices.<sup>[36]</sup> Additionally, it can be used to enhance the merits and further excavate the potential capabilities of other versatile metamaterials.

## Supporting Information

Supporting Information is available from the Wiley Online Library or from the author.

## Acknowledgements

The authors would like to acknowledge the financial support from the National Natural Science Foundation of China (nos. 11622214, 11472027, and 11202012) and the Program for New Century Excellent Talents in University (no. NCET-13-0021).

## Conflict of Interest

The authors declare no conflict of interest.

## Keywords

deformation, metamaterials, pixelation, programmability, shape-reconfigurability

Received: January 23, 2019

Revised: April 7, 2019

Published online: May 9, 2019

- [1] K. Bertoldi, V. Vitelli, J. Christensen, M. van Hecke, *Nat. Rev. Mater.* **2017**, *2*, 17066.
- [2] X. Li, H. Gao, *Nat. Mater.* **2016**, *15*, 373.
- [3] X. Yu, J. Zhou, H. Liang, Z. Jiang, L. Wu, *Prog. Mater. Sci.* **2018**, *94*, 114.
- [4] T. Frenzel, M. Kadic, M. Wegener, *Science* **2017**, *358*, 1072.
- [5] J. I. Lipton, R. MacCurdy, Z. Manchester, L. Chin, D. Cellucci, D. Rus, *Science* **2018**, *360*, 632.
- [6] C. Coulais, D. Sounas, A. Alù, *Nature* **2017**, *542*, 461.
- [7] Z. Zhai, Y. Wang, H. Jiang, *Proc. Natl. Acad. Sci. USA* **2018**, *115*, 2032.

- [8] T. A. Hewage, K. L. Alderson, A. Alderson, F. Scarpa, *Adv. Mater.* **2016**, *28*, 10323.
- [9] Z. G. Nicolaou, A. E. Motter, *Nat. Mater.* **2012**, *11*, 608.
- [10] J. Qu, A. Gerber, F. Mayer, M. Kadic, M. Wegener, *Phys. Rev. X* **2017**, *7*, 041060.
- [11] B. Haghpanah, L. Salari-Sharif, P. Pourrajab, J. Hopkins, L. Valdevit, *Adv. Mater.* **2016**, *28*, 7915.
- [12] Y. Kim, H. Yuk, R. Zhao, S. A. Chester, X. Zhao, *Nature* **2018**, *558*, 274.
- [13] J. L. Silverberg, A. A. Evans, L. McLeod, R. C. Hayward, T. Hull, C. D. Santangelo, I. Cohen, *Science* **2014**, *345*, 647.
- [14] C. Coulais, E. Teomy, K. de Reus, Y. Shokef, M. van Hecke, *Nature* **2016**, *535*, 529.
- [15] N. B. Swift, B.-K. Hsiung, E. B. Kennedy, K.-T. Tan, *J. Mech. Behav. Biomed. Mater.* **2016**, *61*, 271.
- [16] J. F. Vincent, P. Owers, *J. Zool.* **1986**, *210*, 55.
- [17] C. Findeisen, J. Hohe, M. Kadic, P. Gumbsch, *J. Mech. Phys. Solids* **2017**, *102*, 151.
- [18] G. Puglisi, L. Truskinovsky, *J. Mech. Phys. Solids* **2000**, *48*, 1.
- [19] S. Shan, S. H. Kang, J. R. Raney, P. Wang, L. Fang, F. Candido, J. A. Lewis, K. Bertoldi, *Adv. Mater.* **2015**, *27*, 4296.
- [20] T. Frenzel, C. Findeisen, M. Kadic, P. Gumbsch, M. Wegener, *Adv. Mater.* **2016**, *28*, 5865.
- [21] M. Caruel, L. Truskinovsky, *J. Mech. Phys. Solids* **2017**, *109*, 117.
- [22] Q. Ge, H. J. Qi, M. L. Dunn, *Appl. Phys. Lett.* **2013**, *103*, 131901.
- [23] Q. Zhao, H. J. Qi, T. Xie, *Prog. Polym. Sci.* **2015**, *49–50*, 79.
- [24] J. T. Overvelde, T. A. De Jong, Y. Shevchenko, S. A. Becerra, G. M. Whitesides, J. C. Weaver, C. Hoberman, K. Bertoldi, *Nat. Commun.* **2016**, *7*, 10929.
- [25] J. A. Faber, A. F. Arrieta, A. R. Studart, *Science* **2018**, *359*, 1386.
- [26] E. T. Filipov, T. Tachi, G. H. Paulino, *Proc. Natl. Acad. Sci. USA* **2015**, *112*, 12321.
- [27] J. L. Silverberg, J.-H. Na, A. A. Evans, B. Liu, T. C. Hull, C. D. Santangelo, R. J. Lang, R. C. Hayward, I. Cohen, *Nat. Mater.* **2015**, *14*, 389.
- [28] Z. You, *Science* **2014**, *345*, 623.
- [29] H. Fang, S. C. A. Chu, Y. Xia, K. W. Wang, *Adv. Mater.* **2018**, *30*, 1706311.
- [30] I. S. Sokolnikoff, *Mathematical Theory of Elasticity*, McGraw-Hill Book Company, New York **1956**.
- [31] I. Malik, M. Mirkhalaf, F. Barthelat, *J. Mech. Phys. Solids* **2017**, *102*, 224.
- [32] A. Rafsanjani, D. Pasini, *Extreme Mech. Lett.* **2016**, *9*, 291.
- [33] F. Fraternali, T. Blesgen, A. Amendola, C. Daraio, *J. Mech. Phys. Solids* **2011**, *59*, 89.
- [34] S. Maeda, Y. Hara, T. Sakai, R. Yoshida, S. Hashimoto, *Adv. Mater.* **2007**, *19*, 3480.
- [35] C. Keplinger, J.-Y. Sun, C. C. Foo, P. Rothemund, G. M. Whitesides, Z. Suo, *Science* **2013**, *341*, 984.
- [36] H. Yasuda, T. Tachi, M. Lee, J. Yang, *Nat. Commun.* **2017**, *8*, 962.